Novel Compacting Grounding System for Mitigating Ground Potential Rise and Backflashovers

J. E. Guevara Asorza, Walter L. M. Azevedo, J. Pissolato Filho

***Abstract*—Proper grounding is essential for mitigating the risks associated with lightning strikes on Overhead Transmission Lines (OHTL), as it helps protect equipment and ensures system reliability. To achieve this, various grounding system (G.S) designs can be implemented. This paper introduces two new alternatives to the Conventional grounding system (CGS): the "Compact Grounding System" (CMGS) and the "Improved Compact Grounding System" (IGS). These designs are intended to use a smaller installation area while delivering similar or even superior performance, particularly in managing Ground Potential Rise (GPR) and minimizing backflashovers during lightning strikes. Among the evaluated systems, the IGS demonstrated the best overall performance, achieving lower GPR and reducing the occurrence of backflashovers, even in challenging conditions with high-resistivity soils and high values of lightning current. The study highlights the potential of these innovative designs to improve the safety and efficiency of power transmission systems, especially in space-constrained and high-resistivity environments.**

***Keywords*—Ground potential rise, transient analysis, grounding system, backflashover, lightning study**

NOMENCLATURE

BF	Backflashover
CGS	Conventional Ground System
CMGS	Compact Grounding System
EHS	Extra High Strength
GPR	Ground Potential Rise
GS	Grounding System
IGS	Improved Compact Grounding System
ULM	Universal Line Model
WF	Waveform

I. INTRODUCTION

THE protection of power systems against lightning strikes is a well-researched field, as these systems are particularly vulnerable to such events. If the lightning current is not properly dissipated, it can cause damaging overvoltages, including backflashovers [1], which may lead to power outages, equipment damage, and high Ground Potential Rise (GPR). To mitigate these risks, the design of an effective grounding system (G.S) is essential. The G.S is fundamental in safely dissipating high currents generated by lightning strikes, ensuring the safe and reliable operation of power systems.

There are no specific rules for designing a G.S., but certain criteria must be met. In steady-state conditions, the grounding system should maintain an impedance of 25 Ω or lower [2]. Additionally, it must ensure that step and touch voltages remain within safe limits, particularly in populated areas, during fault conditions [3]. Space limitations can also present significant challenges, especially in urban environments where the available area is often restricted. For transmission towers, counterpoise ground wires are frequently employed as a key component of the grounding system [4]. However, in regions with high-resistivity soils, using very long counterpoise wires may be necessary, which is often impractical, particularly when transmission lines are situated near roads, rivers, or other natural barriers. In these cases, such features make it impossible to construct long counterpoise wires, as these obstacles act as barriers to installation.

In this context, the main contribution of this study is to propose a new grounding system configuration with its improved version and evaluate its transient performance compared to conventional counterpoise wires while also ensuring compliance with steady state requirements. This new configuration offers the advantage of requiring a significantly smaller installation area. To perform this comparison, Maxwell's equations for each G.S configuration were solved using the full-wave electromagnetic software FEKO® [5], which employs the method of moments for precise impedance calculations across a range of frequencies. Once the impedance values were determined, Ground Potential Rise (GPR) and backflashover potential were calculated for a 220 kV transmission line using PSCAD® [6], considering various lightning current scenarios and analyzing backflashover behavior.

II. NEW GROUNDING SYSTEM

This work proposes two new grounding system topologies, referred to as Compact grounding system (CMGS) and Improved Compact grounding system (IGS). In addition, a comparison between these new grounding designs and a Conventional counterpoised grounding system (CGS) is made. The configurations of each G.S are shown in Fig.1, where:

- L_{CP} is the counterpoise wire;

This paper was supported by the São Paulo Research Foundation (FAPESP) grants: 2021/11258-5, 2023/05066-1 and 2024/14472-6 and by the Coordenação de Aperfeiçoamento de Pessoal de Nível Superior (CAPES)-Finance code 001. J. E. Guevara Asorza is with the University of Campinas - UNICAMP, Campinas, Brazil, (e-mail: j272296@dac.unicamp.br). W. L. Azevedo is with the University of Campinas - UNICAMP, Campinas, Brazil (e-mail of corresponding author: w157573@dac.unicamp.br). J. P. Filho is with the University of Campinas - UNICAMP, Campinas, Brazil, (e-mail: pisso@unicamp.br).

Paper submitted to the International Conference on Power Systems Transients (IPST2025) in Guadalajara, Mexico, June 8-12, 2025.

- $L_v = 2.4$ m is vertical rod length;
- $L_{QD} = 10$ m is the side length of the main square;
- $L_x = 2$ m is the distance between the internal red square (side D_{qi}), and the external green square (side D_{qe}).
- L_c is the counterpoise wire for the CMGS.

Every grounding system is buried at a depth of 0.6 m and made of copper. Other parameters, which vary with soil resistivity, are detailed in the Table I. The soil electric resistivity and permittivity were modeled using the approach proposed by CIGRE [7]. Four frequency electrical resistivities were considered: 2000, 5000, 7000, and 10000 Ωm.

The grounding impedance of each G.S is calculated using the *full-wave approach* FEKO software, applying the Method of Moments (MoM) [5]. In the simulation, the soil is modeled as a dielectric medium, with its resistivity and permittivity defined by CIGRE models. The G.S is designed in FEKO and buried in this dielectric medium, incorporating the soil's electrical properties as per CIGRE. The simulation procedure follows the methodology described in [8]. Points A, B, C, and D represent the locations of the voltage sources used in the simulations. These points also serve as the connection points between the G.S. and the transmission tower. The voltage sources apply a voltage difference of $V_s(j\omega) = 1\angle 0°$, V. Then, the induced current $I_{\text{in}}(j\omega)$ flowing into the G.S. through the injection point is calculated by solving Maxwell's equations with MoM. Finally, the grounding impedance is then computed by FEKO as follows

$$Z(j\omega) = \frac{V_s(j\omega)}{I_{\text{in}}(j\omega)}, \tag{1}$$

where ω is the angular frequency, $V_s(j\omega)$ and $I_{\text{in}}(j\omega)$ are the frequency-domain quantities representing the phasor of the potential developed at the point and the injected current at that point, respectively.

The conventional grounding's counterpoise length (L_{CP}) was calculated to maintain an impedance of less than or equal to 25 Ω at low-frequency, around 100 Hz. The L_{CP} values for each studied case are provided in Table I. The CMGS design was developed with the primary constraint that the total side length of the system cannot exceed 25 m, as shown in Fig.1, which represents the right of way corridor for the 220 kV transmission line. As a result of this limitation, L_q can only have a maximum value of 5 m. To ensure a fair comparison between both G.S, the design steps for the CMGS are as follows:

1) The total length of copper cable for the CGS is distributed among four smaller squares of side length L_q, each connected to the main square (side length L_{QD}) by segments of length D_x. These connections are represented by the black lines in Fig. 1.
2) A diagonal copper cable D_s is added to each smaller square to improve performance, as shown by the yellow line in Fig. 1.
3) If any copper wire remains, it is then used to form an internal square (side length D_{qi}), as represented by the red lines in Fig. 1.
4) Further remaining wire is applied to the external square (side length D_{qe}), indicated by the green lines in Fig. 1.

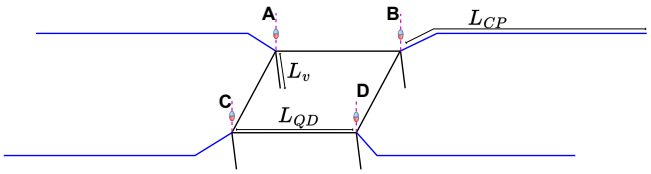

(a) Conventional counterpoised G.S (CGS).

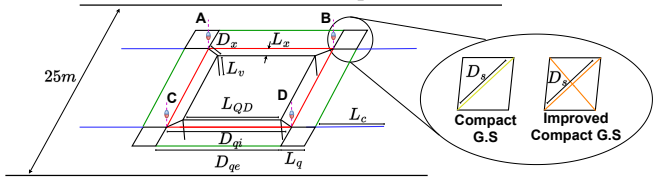

(b) Compact (CMGS) and Improved Compact (IGS) G.S.

Fig. 1: Grounding systems used in this work.

5) If more wire is still available, it is then distributed along four horizontal rods (L_c), represented by blue lines in Fig. 1.
6) For IGS, four additional diagonal cables (D_s) are added to each square, as shown in orange line in Fig. 1.

III. Modeling Power Systems Elements

A. Computing electrical parameters for an OHTL

In the literature, two full-wave formulations exist [9], [10], developed using the electric scalar potential and the magnetic vector potential. These formulations are referred as the potential formulation and the voltage formulation. The first establishes a remote ground for potential reference, while the latter calculates the voltage between the overhead conductor and the soil's surface. The difference in results between these formulations in a lightning study is evident [11]. Therefore, in this study, we will employ the latter formulation.

B. Tower model

The revised Jordan's formula was employed to calculate the tower surge impedance. This formula approximates the apparent propagation speed along the tower as about 80% of the speed of light, as detailed in [12], considering the tower sections and cross arms. According to [13], this model aligns well with the Hybrid Electromagnetic Model (HEM). In this study, we determined the equivalent impedance values, Zeq_i, using the following expressions:

$$Z_{i,i} = Z_{ii} = 60\, ln\left(\frac{4h}{r}\right) - 60, \tag{2}$$

$$Z_{i,j} = 60\, ln\left(\frac{2h + \sqrt{4h^2 + d_{ij}^2}}{d_{ij}^2}\right) + 30\frac{d}{h} - 60\sqrt{1 + \frac{d_{ij}^2}{4h^2}}, \tag{3}$$

$$Zeq_i = \frac{Z_{i1} + Z_{i2} + Z_{i3} + ... + Z_{in}}{n}, \tag{4}$$

where h represents the height in meters, d_{ij} denotes the distance in meters between conductors i and j (main chords), r stands for the radius of the main chord, and n indicates

the number of main chords. The calculated values are Zeq_4 = 217.69 Ω, Zeq_3 = 215.38 Ω, Zeq_2 = 210.28 Ω and Zeq_1 = 131.7 Ω. The impedance values for the cross arms, including those supporting the shield wires, are 173.03 Ω·m.

C. Insulator string model

In this research, the simplest model for the insulator string was utilized, the voltage-time (VT) curve. This model focuses solely on the length of the insulator string to assess its voltage withstand capability (V_{FO}), as described in [14]. A back flashover will likely occur if a lightning overvoltage exceeds the V-T curve.

D. Lightning current model

In this work, the lightning waveform was considered as a combination of seven Heidler functions described in [15]. The lightning waveform is expressed as follows:

$$i(t) = \sum_{k=1}^{N} \frac{I_{0k}}{\eta_k} \frac{(t/\tau_{1k})^{n_k}}{1+(t/\tau_{1k})^{n_k}} e^{(-t/\tau_{2k})}, \quad (5)$$

$$\eta_k = \exp\left[-\left(\frac{\tau_{1k}}{\tau_{2k}}\right)\left(n_k \frac{\tau_{2k}}{\tau_{1k}}\right)^{\frac{1}{n_k}}\right], \quad (6)$$

where I_{0k} regulates the amplitude, τ_{1k} represents the time constant related to the front time, τ_{2k} is the decay time constant, η_k is the amplitude correction factor, and n_k is the exponent that dictates the slope of each component k.

IV. Results

This section is structured in two parts. The first part presents the grounding impedance of the new G.S in the frequency domain, considering four different values of electrical resistivity of the soil, 2000, 5000, 7500, and 10000 Ω·m, according to the formulation proposed by CIGRE 781 [7]. These impedances are computed using the software FEKO for each electrical resistivity, following the methodology indicated in the Section II. The second section calculates the number of backflashover and the GPR when lightning strikes the tower through the shield wire. These last simulations were done in PSCAD®.

A. Grounding system impedance

For this analysis, it was considered a grounding system for an OHTL single-circuit at 220 kV. According to the methodology indicated in Section II, Table I presents the dimensions of the new grounding systems and the counterpoise length of the CGS.

The dimensions for the CGS were calculated to ensure that its steady state electrical impedance remains at 25 Ω or lower. The CMGS was designed based on the total length of the CGS and the steady state requirements, the IGS is designed with more copper for enhanced performance. At a ground resistivity of 2000 Ω·m, the CMGS requires 17% more copper than the conventional counterpoise design, while the IGS requires 34% more. However, this percentage of additional copper requirement decreases as soil resistivity increases. For example, at a resistivity of 10000 Ω·m, the copper requirements are reduced to 8.3% and 16.6% for the CMGS and IGS, respectively. This trend highlights the improved efficiency of these designs in high-resistivity environments. Considering the dimensions presented in the Table I, the Figs. 2 and 3 present the magnitude and angle of the grounding impedance for the studied cases.

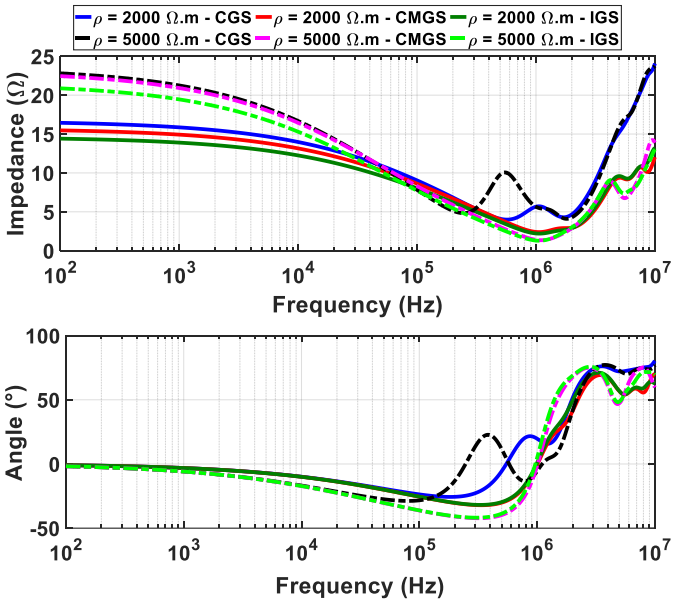

Fig. 2: (a) Magnitude and (b) angle of the grounding impedance when ρ = 2000 Ω.m and 5000 Ω.m

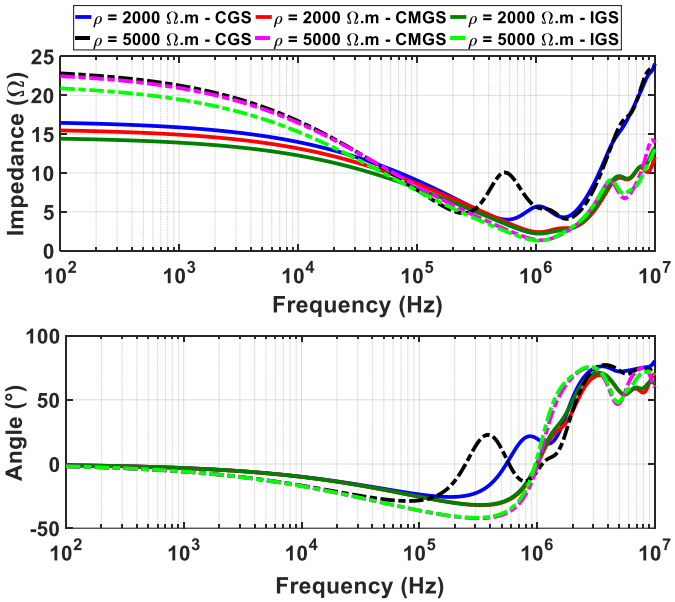

Fig. 3: (a) Magnitude and (b) angle of the grounding impedance when ρ = 7500 Ω.m and 10000 Ω.m

Figs. 2 and 3 show the grounding impedances calculated by FEKO for each proposed G.S. and the four studied soil resistivities. The top part of Fig. 2 shows the magnitude of the grounding impedance considering two values of ground electrical resistivity: 2000 Ω·m and 5000 Ω·m. In the steady state, for both resistivity values, the impedance magnitude for the CGS is higher than that of the CMGS and IGS. However,

TABLE I: Grounding system dimensions for each ground electrical resistivity

Ground electrical resistivity (Ω.m)	Counterpoise length CGS (m)	Dimensions of the CMGS and IGS (m)	Total length CGS (m)	Total length CMGS (m)	Total length IGS (m)
2000	15	Square side (L_q): 3.043 Diagonal of the square (D_s): 4.303 Distance between squares - Internal side (D_{qi}): - Distance between squares - External side (D_{qe}): - Length of external counterpoise (L_c): -	100	117.21	134.43
5000	35	Square side (L_q): 4.054 Diagonal of the square (D_s): 5.733 Distance between squares - Internal side (D_{qi}): 14 Distance between squares - External side (D_{qe}): - Length of external counterpoise (L_c): -	180	195.11	218.04
7500	55	Square side (L_q): 5 Diagonal of the square (D_s): 7.071 Distance between squares - Internal side (D_{qi}): 14 Distance between squares - External side (D_{qe}): 14 Length of external counterpoise (L_c): 4.17	260	288.28	316.56
10000	75	Square side (L_{QD}): 5 Diagonal of the square (D_s): 7.071 Distance between squares - Internal side (D_{qi}): 14 Distance between squares - External side (D_{qe}): 14 Length of external counterpoise (L_c): 24.17	340	368.28	396.56

as frequency increases, the impedance of the CGS decreases. For 5000 Ω·m, at around 35 kHz, the impedance magnitude of the CGS becomes lower than that of the CMGS, but remains higher than that of the IGS. At 110 kHz, the impedance of the CGS is lower than that of the IGS until approximately 240 kHz, where the impedance starts to increase again, surpassing that of the IGS, and at 270 kHz, it also surpasses the impedance of the CMGS. Similarly, for 2000 Ω·m, the impedance magnitude of the CGS becomes lower than that of the CMGS, but between 28 kHz and 47 kHz, this relationship reverses, with the CGS showing a higher impedance. Beyond 47 kHz, the CGS impedance increases once more. For this value of ground resistivity, the IGS consistently maintains a lower impedance than the other two grounding systems. This behavior is also observed for a ground resistivity of 7500 Ω·m, as shown in Fig. 3. However, for a ground resistivity of 10000 Ω·m, the CMGS has a higher grounding impedance than the CGS by 0.38 Ω at low frequencies, up to about 127 kHz. The three G.S exhibit capacitive behavior at low frequencies, shifting to inductive behavior at higher frequencies. For 2000 Ω·m, this transition occurs at 573 kHz for the CGS, and nearly 1 MHz for the IGS. The longer counterpoise length of the CGS contributes to this shift by introducing more inductance, which counteracts its capacitive effects. This shift in the frequency range where atmospheric discharges operate can negatively impact lightning performance, increasing GPR and backflashovers. To mitigate this, it is preferable that the change occurs at higher frequencies, which is challenging for high-resistivity soils. For instance, at 10000 Ω·m, the transition between capacitive and inductive behavior occurs at 100 kHz, while the CMGS and IGS maintain a more favorable transition above 800 kHz.

B. Backflashover and GPR study

The OHTL used in this work features an extra-high-strength (EHS) wire to support the aluminum alloy conductor (AAAC 1000 kcmil). Furthermore, the OHTL has an optical ground wire (OPGW) to provide communication along the line and a grounding path to protect against lightning discharges. Detailed data for the OHTL are provided in Table II, and the location of the tower conductors in Fig. 4.

TABLE II: Data for the OHTL at 220 kV

Description	Unit	Value
Type of conductor	-	AAAC 1000 kcmil
Conductor external diameter	mm	29.27
Conductor internal diameter	mm	0.0
Conductor resistance in DC - 20°C	Ω/km	0.06627
Type of EHS	-	EHS 7/16
EHS external diameter	mm	11.11
EHS Resistence in DC - 20°C	Ω/km	2.815
Type of OPGW	-	AlumaCore - AFL
OPGW external diameter	mm	14.5
OPGW internal diameter	mm	9
OPGW Resistence in DC - 20°C	Ω/km	0.441
Average span	m	430

The same four values of ground electrical resistivity and three G.S discussed in subsection IV-A were considered. Furthermore, four lightning waveforms (WF) were considered, adapted from [16], which parameters are presented in Table III. In order to represent these current waveforms accurately, (5) and (6) were employed, and their parameters were iteratively adjusted through the self-correcting routine described in [17].

TABLE III: Lightning waveforms (WF) employed

Parameter	WF 1	WF 2	WF 3	WF 4	WF 5
$Ip1$ (kA)	76.61	95.76	114.91	134.06	153.21
$Ip2$ (kA)	85.05	105.69	126.22	146.66	167.02
$T30$ (μs)	7.21	8.57	9.87	11.13	12.34
$T10$ (μs)	8.93	9.92	10.81	11.63	12.39
$T50$ (μs)	56.2	56.2	56.2	56.2	56.2

Considering the input data presented in Table II and tower silhouette in Fig. 4, the electrical parameters for the OHTL were calculated using the voltage formulation, as it was indicated in subsection III-A, considering the frequency dependence of the soil with the formulations recommended by CIGRE 781 [18]. Then, the series impedance and shunt

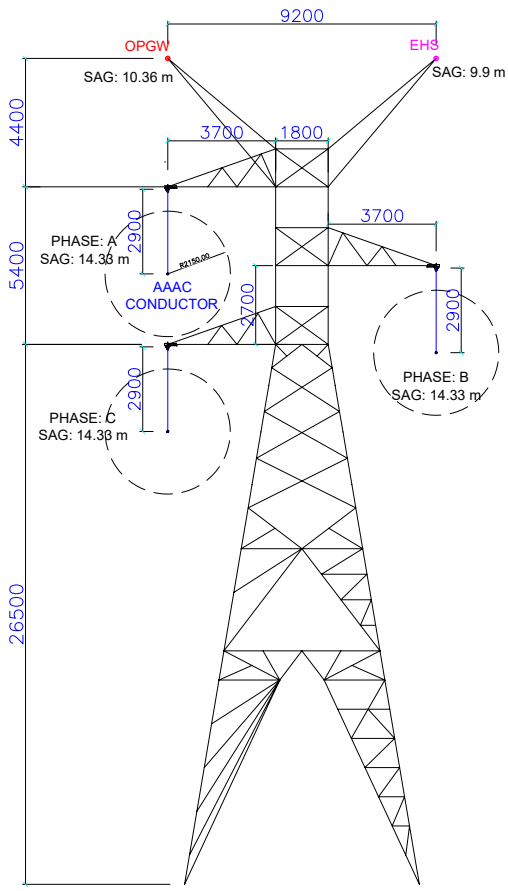

Fig. 4: Layout of the 220-kV tower.

admittance in the frequency domain were calculated in MATLAB and subsequently imported into PSCAD® through the YZ routine integrated within the software, as it is indicated in [19]. PSCAD® incorporates the Universal Line Model (ULM) [20], offering a comprehensive and accurate frequency-dependent model for OHTL by fitting propagation matrices H and characteristic admittance Yc in the phase domain. Within PSCAD®, the transient response of the OHTL was simulated considering the WF presented in Table III.

Key aspects from CIGRE 839 [17] were considered for a comprehensive lightning analysis, including tower surge impedance, lightning stroke modeling, number of towers, insulator string representation, and the power-frequency source with varying phase angles. All system components were implemented in PSCAD®, as illustrated in Fig. 5. The power system modeled in PSCAD® comprises five distinct transmission towers, each equipped with its grounding system. The lightning strike is applied to the central tower via the OPGW shield wire at point CG_1. Each span, denoted as Tr_i, is represented using the UL model, incorporating the frequency-domain electrical parameters— the series impedance and shunt admittance matrices—previously calculated and exported via the YZ routine. The towers were modeled by Bergeron [21] with surge impedance, propagation velocity and length [22], [23], as shown in Fig. 6.

The insulator string length, measured from the energized to the de-energized section, is 2.10 m, represented as block diagrams in PSCAD is [23]. Additionally, to account for the voltage waveform of the 60 Hz power-frequency source, it is necessary to estimate the time required for this waveform to reach the tower under analysis. In this context, considering a 10 km segment of OHTL located near the power source, Tr_6, the propagation time is approximately 39 μs. Consequently, the lightning source was configured with a 40 μs delay to ensure that the voltage wave produced by the power source is already present at the exact location when the lightning strikes the tower. A shorter line segment was deliberately avoided, as lengths below 10 km could introduce artificial reflections, potentially compromising the accuracy of the transient analysis. At the opposite end of the implemented system, an OHTL modeled as a reflectionless line—properly from PSCAD—was included to eliminate artificial reflections from that boundary. This approach, however, was not applied to the OHTL segment connected to Tr_6, since doing so would exclude the inclusion of the voltage waveform associated with the 60 Hz power-frequency source, which is essential for accurately representing the steady-state operating conditions before the lightning event. Furthermore, the power frequency source angles were varied in increments of 60°, ranging from 0° to 360°. This study observed the highest overvoltages on the insulator strings when the power frequency source angle was set to 60°. At this angle, the highest voltage was recorded in phase A (163.34 kV), followed by phase B (0 kV), and finally phase C (-163.34 kV).

The frequency-dependent grounding impedance (both magnitude and phase) calculated in FEKO was exported to PSCAD/EMTDC using the Frequency Dependent Network Equivalent (FDNE) tool. This tool approximates the frequency response (in this case, the grounding impedance) via vector fitting to create a rational function representation [24]. Following the approach described in [25], this enables constructing an equivalent frequency-dependent network model. For this study, the maximum order of fitting was 20, while the maximum fitting error was 0.5 %.

Figures 7 and 8 illustrate the results of the GPR for the four values of ground electrical resistivity, the three grounding systems and the five lightning WF analyzed. Fig. 7 illustrates the GPR behavior of the three grounding systems for varying lightning WF at ground resistivities of 2000 Ω·m and 5000 Ω·m. For 2000 Ω·m, the peak GPR values generated by the CGS are higher than those of the CMGS and IGS, with the greatest difference occurring when waveform WF4 is applied. For this WF, the difference of peak GPR value between the CGS and the CMGS is 60 kV (4.95%), while the difference between the CGS and IGS is 121.6 kV (9.91%). Furthermore, when WF5 strikes the overhead transmission line (OHTL), the GPR of the CGS shows a minor disturbance at 31 μs, indicating the occurrence of a backflashover. In the case of 5000 Ω·m, similar to the 2000 Ω·m scenario, the highest GPR peak values are observed with the CGS. Here, the greatest difference is noted with WF2, where a difference of 99 kV (8.94%) is recorded when using the CMGS, and a difference of 153 kV (13.81%) when the IGS is employed. A disturbance is also observed in the GPR for all three grounding systems between 30 and 33 μs when WF5 strikes the OHTL, indicating

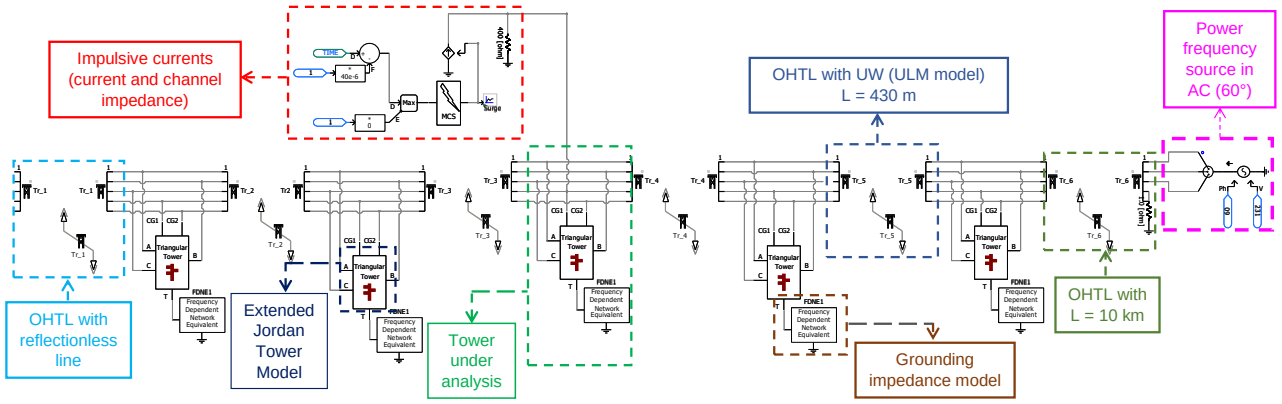

Fig. 5: System implemented in PSCAD®

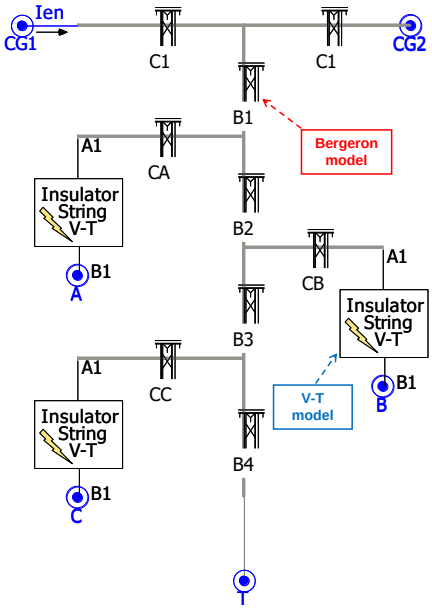

Fig. 6: Tower modeled in PSCAD

that a backflashover occurs for each grounding system.

For the resistivities presented in Fig. 8, the CMGS generated higher GPR values than both the CMGS and IGS. In contrast, the CGS produced higher GPR values than the IGS; however, this difference diminishes as electrical resistivity increases. Considering the WF5 with a ground electrical resistivity of 7500 Ω·m, a backflashover occurs for all three grounding systems. However, when the resistivity increases to 10000 Ω·m, a backflashover occurs only in the CMGS. For more information about the lightning performance during backflashovers, Figs. 9 to 12 illustrate the overvoltage on the insulator string specifically for WF5, where backflashover events are observed.

Figure 9 shows the overvoltage on the insulator string for a ground electrical resistivity of 2000 Ω·m across the three grounding systems. The GPR analysis indicates that a backflashover occurs only for the CMGS. As the resistivity increases, backflashovers are observed in all three scenarios, as shown in Fig. 10. However, these events occur on different occasions, indicating that the critical currents required to generate backflashovers differ. For the 5000 Ω·m resistivity,

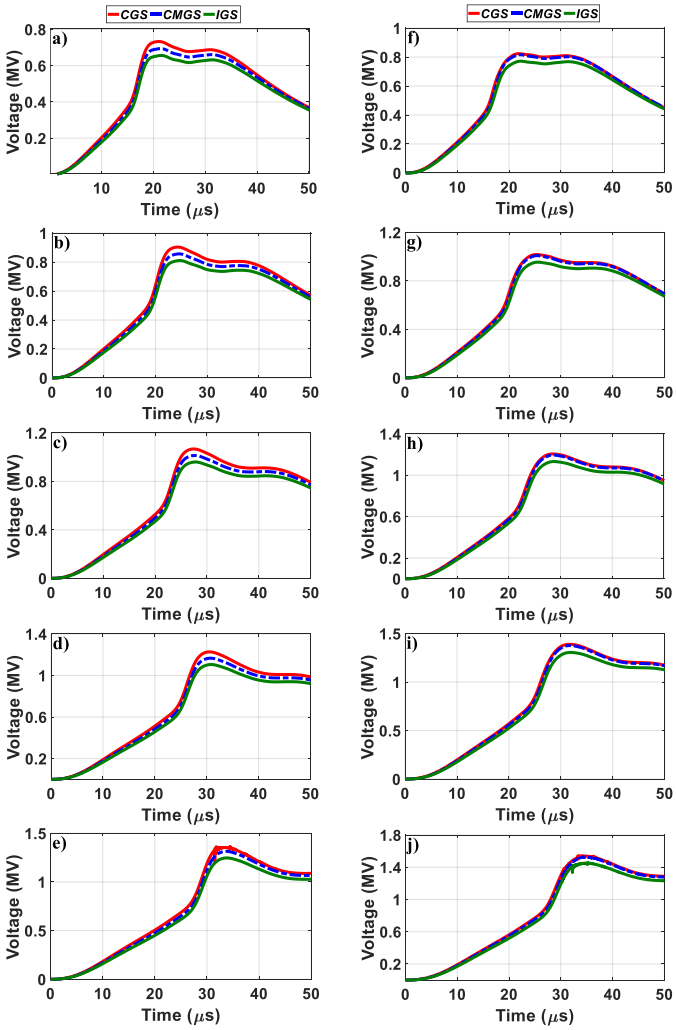

Fig. 7: GPR results for 2000 Ω.m (left side) and 5000 Ω.m (Right side) , (a,f) WF1, (b,g) WF2, (c,h) WF3, (d,i) WF4, (e,j) WF5.

the critical currents are 140.39 kA for the CGS, 143.08 kA for the CMGS, and 149.28 kA for the IGS. These values represent the currents measured at the moment the backflashover occurs. For a resistivity of 7500 Ω·m, the critical currents are 151 kA, 149.87 kA, and 151.5 kA for the CGS, CMGS and IGS, respectively. This indicates that the cumulative probability of back flashovers decreases when the IGS is employed.

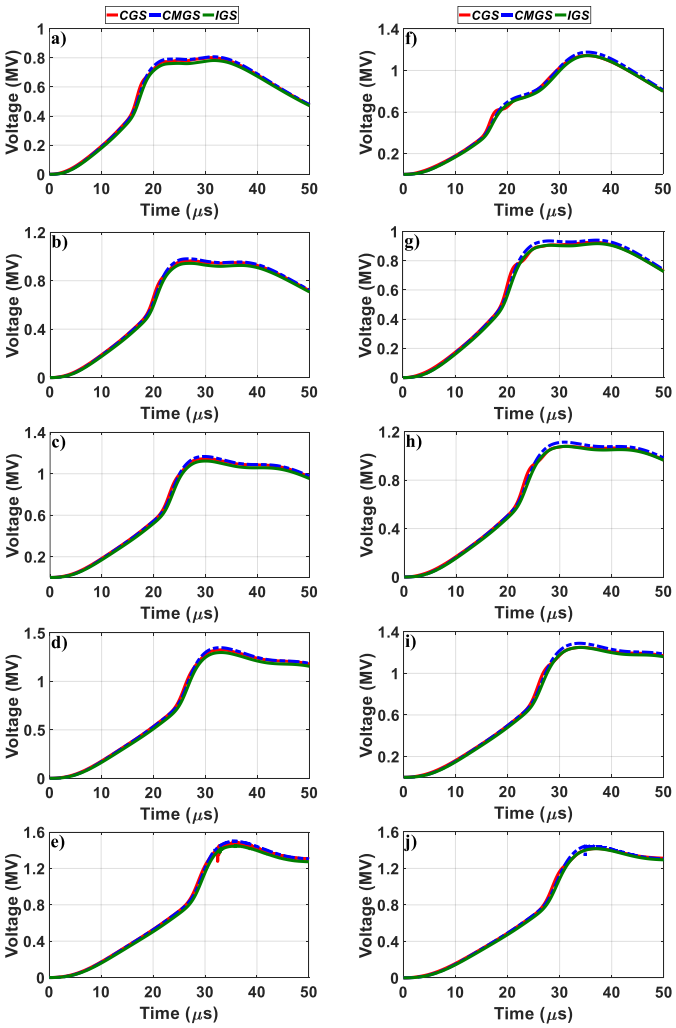

Fig. 8: GPR results for 7500 Ω.m (left side) and 10000 Ω.m (Right side) , (a,f) WF1, (b,g) WF2, (c,h) WF3, (d,i) WF4, (e,j) WF5.

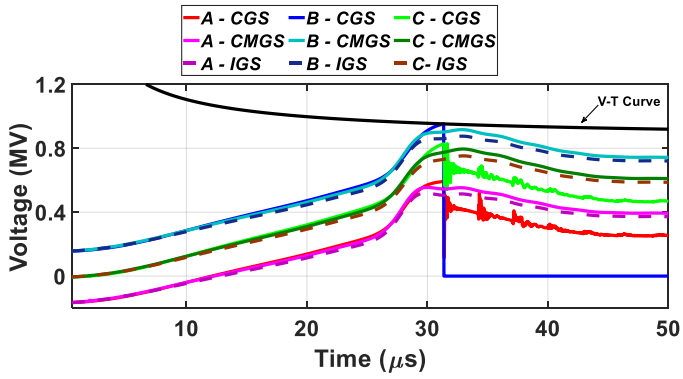

Fig. 9: Voltages across the insulator string for 2000 Ω.m and WF5

Furthermore, when the ground electrical resistivity reaches 10000 Ω·m, a backflashover occurs in phase B only with the CMGS. Table IV summarizes the results of the GPR peak values and the occurrences of backflashovers in the OHTL.

Table IV indicates that, for the electrical resistivity of 2000 and 5000 Ω·m, the CMGS and IGS has a better performance in GPR and backflashover. Additionally, when

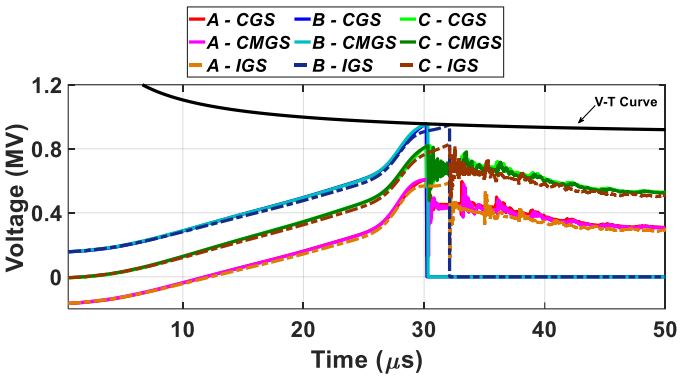

Fig. 10: Voltages across the insulator string for 5000 Ω.m and WF5

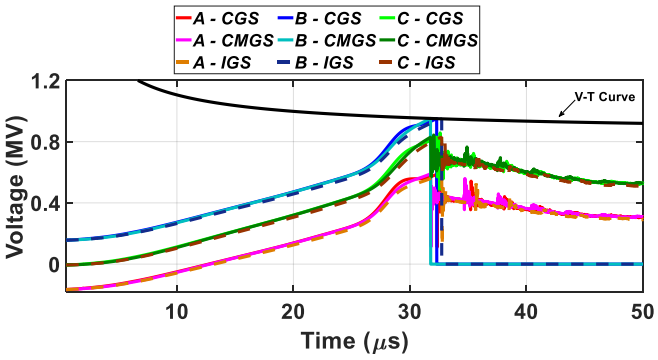

Fig. 11: Voltages across the insulator string for 7500 Ω.m and WF5

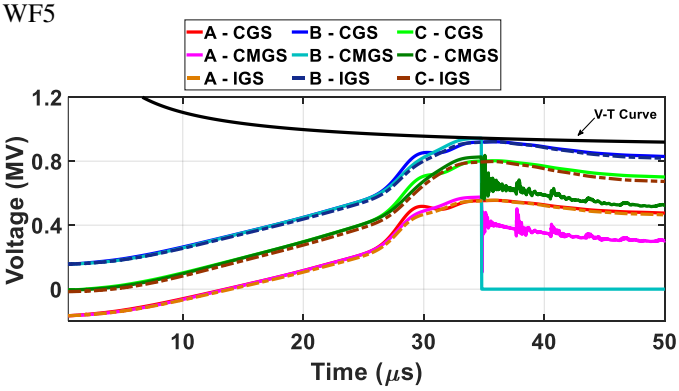

Fig. 12: Voltages across the insulator string for 10000 Ω.m and WF5

TABLE IV: Results of maximum GPR and Backflashover (BF)

WF	Ground Electrical Resisitivity (Ω.m)	CGS		CMGS		IGS	
		Maximum GPR (MV)	BF	Maximum GPR (MV)	BF	Maximum GPR (MV)	BF
1	2000	0.733	-	0.694	-	0.656	-
	5000	0.824	-	0.816	-	0.772	-
	7500	0.801	-	0.807	-	0.781	-
	10000	1.143	-	1.176	-	1.143	-
2	2000	0.903	-	0.856	-	0.811	-
	5000	1.107	-	1.008	-	0.954	-
	7500	0.965	-	0.981	-	0.944	-
	10000	0.926	-	0.941	-	0.917	-
3	2000	1.068	-	1.014	-	0.960	-
	5000	1.206	-	1.195	-	1.132	-
	7500	1.147	-	1.166	-	1.123	-
	10000	1.089	-	1.114	-	1.079	-
4	2000	1.227	-	1.166	-	1.105	-
	5000	1.389	-	1.377	-	1.306	-
	7500	1.325	-	1.347	-	1.298	-
	10000	1.250	-	1.289	-	1.249	-
5	2000	1.363	B	1.315	-	1.247	-
	5000	1.540	B	1.527	B	1.46	B
	7500	1.496	B	1.501	B	1.452	B
	10000	1.418	-	1.465	B	1.416	-

the electrical resistivity increases to 7500 Ω·m, the CMGS outperforms the CGS only in cases where the lightning discharge corresponds to WF1 and WF2. These waveforms have the largest frequency spectrum between the studied cases. Then, when the atmospheric discharge increases in magnitude and decreases frequency operation, the CGS has a better performance than the CMGS; however, the IGS still has the best performance, even when the electrical resistivity increases to 10000 Ω.m.

V. Conclusions

This paper presents a novel grounding system referred to as the "Compact grounding system" (CMGS) along with an enhanced version known as the "Improved Compact grounding system" (IGS). The primary aim of these new grounding systems is to be applicable in areas where it is not feasible to install long counterpoises typical of a "Conventional grounding system" (CGS), while maintaining at least the same resistance value in steady-state conditions and improving performance during lightning events. The first part of the results introduces the novel grounding systems, detailing their behavior in the frequency domain, the design methodology, and the factors influencing their performance. The design strategy involves utilizing the counterpoise dimensions from the CGS to create these new systems. The dimensions are strongly dependent on the electrical resistivity of the ground, which is analyzed across four different values: 2000, 5000, 7500, and 10000 Ω·m. The results reveal that the CGS transitions from a capacitive to an inductive behavior, increasing grounding impedance magnitude at high frequencies. This transition occurs earlier for the CGS than for the CMGS and IGS, making the transient performance of CGS worse than the other two proposed grounding systems. The GPR, overvoltages, and backflashover events for five lightning waveforms were also analyzed. The findings indicate that the CMGS outperforms the CGS at lower electrical resistivities (2000 and 5000 Ω·m). However, this trend reverses at higher resistivity values. Conversely, the IGS demonstrates a superior performance across all electrical resistivity values and lightning waveforms. Finally, although the new grounding systems require slightly more copper, the increase is negligible relative to the overall transmission line cost—especially given the significant performance improvement achieved without demanding additional installation space, a key factor in constrained environments.

References

[1] R. Batista, P. Louro, and J. Paulino, "Lightning performance of a critical path from a 230-kv transmission line with grounding composed by deep vertical electrodes," *Electric Power Systems Research*, vol. 195, p. 107165, 2021.

[2] N. G. Bingel III, C. C. Bleakley, A. L. Clapp, J. H. Dagenhart, M. A. Konz, L. E. Gaunt, M. B. Gunter, and M. F. Jurgemeyer, *2017 NESC(R) Handbook, Eighth Edition*, 2017.

[3] "Ieee guide for safety in ac substation grounding," *IEEE Std 80-2013 (Revision of IEEE Std 80-2000/ Incorporates IEEE Std 80-2013/Cor 1-2015)*, pp. 1–226, 2015.

[4] C. H. Moreira, F. H. Silveira, L. L. Bittencourt, and S. Visacro, "Technical-economic analysis of conventional and non-conventional techniques to improve the lightning performance of transmission lines: Extended counterpoise grounding wires and underbuilt wires," *Electric Power Systems Research*, vol. 214, p. 108805, 2023.

[5] FEKO, "FEKO Altair Engineering Inc.,," [Online]. Available: https://altair.com/feko

[6] PSCAD Simulation Software. Accessed 2023-09-30. [Online]. Available: https://hvdc.ca/pscad

[7] Working Group C4.33, "Impact of soil-parameter frequency dependence on the response of grounding electrodes and on the lightning performance of electrical systems," 2019, CIGRE TB 781.

[8] W. L. M. de Azevedo, A. R. J. De Araújo, and J. Pissolato Filho, "The effect of sandy soil porosity on lightning overvoltages of overhead 138 kv transmission line," *Electric Power Systems Research*, vol. 220, p. 109272, 2023.

[9] A. C. S. Lima, R. A. R. Moura, M. A. O. Schroeder, and M. T. C. de Barros, "Different approaches on modeling of overhead lines with ground displacement currents," in *International Conference on Power Systems Transients (IPST)*, 2017.

[10] J. S. L Colqui, R. A. R Moura, M. A. O Schroeder, J. P. Filho, and S. Kurokawa, "The impact of transmission line modeling on lightning overvoltage," *Energies*, vol. 16, no. 3, 2023.

[11] J. E. Guevara, J. S. L. Colqui, and J. P. Filho, "Analysis of overvoltage and backflashover with different transmission line models," in *SoutheastCon 2024*, 2024, pp. 498–503.

[12] A. De Conti, S. Visacro, A. Soares, and M. Schroeder, "Revision, extension, and validation of jordan's formula to calculate the surge impedance of vertical conductors," *IEEE Transactions on Electromagnetic Compatibility*, vol. 48, no. 3, pp. 530–536, 2006.

[13] F. S. Almeida, F. H. Silveira, A. De Conti, and S. Visacro, "Influence of tower modeling on the assessment of backflashover occurrence on transmission lines due to first negative lightning strokes," *Electric Power Systems Research*, vol. 197, p. 107307, 2021.

[14] "Modeling guidelines for fast front transients," *IEEE Transactions on Power Delivery*, vol. 11, no. 1, pp. 493–506, 1996.

[15] A. De Conti and S. Visacro, "Analytical representation of single- and double-peaked lightning current waveforms," *IEEE Transactions on Electromagnetic Compatibility*, vol. 49, no. 2, pp. 448–451, 2007.

[16] F. H. Silveira and S. Visacro, "Lightning parameters of a tropical region for engineering application: Statistics of 51 flashes measured at morro do cachimbo and expressions for peak current distributions," *IEEE Transactions on Electromagnetic Compatibility*, vol. 62, no. 4, pp. 1186–1191, 2020.

[17] Working Group C4.23, "Procedures for estimating the lightning performance of transmission lines – new aspects," 2021, CIGRE TB 839.

[18] CIGRE Working Group C4.33, "Impact of soil-parameter frequency dependence on the response of grounding electrodes and on the lightning performance of electrical systems," p. 67, 2019.

[19] J. E. G. Asorza, J. S. L. Colqui, F. F. Da Silva, and J. P. Filho, "Lightning response on cable core and sheath in single-circuit underground cable," in *2024 Workshop on Communication Networks and Power Systems (WCNPS)*, 2024, pp. 1–7.

[20] A. Morched, B. Gustavsen, and M. Tartibi, "A universal model for accurate calculation of electromagnetic transients on overhead lines and underground cables," *IEEE Transactions on Power Delivery*, vol. 14, no. 3, pp. 1032–1038, 1999.

[21] J. E. G. Asorza, J. S. Colqui, and J. P. Filho, "Electromechanical analysis of underbuilt wire use in transmission lines," *Electric Power Systems Research*, vol. 240, p. 111282, 2025. [Online]. Available: https://www.sciencedirect.com/science/article/pii/S0378779624011684

[22] N. Zawani, Junainah, Imran, and M. Faizuhar, "Modelling of 132kv overhead transmission lines by using atp/emtp for shielding failure pattern recognition," *Procedia Engineering*, vol. 53, pp. 278–287, 2013, malaysian Technical Universities Conference on Engineering & Technology 2012, MUCET 2012.

[23] M. Qais and U. Khaled, "Evaluation of v–t characteristics caused by lightning strokes at different locations along transmission lines," *Journal of King Saud University - Engineering Sciences*, vol. 30, no. 2, pp. 150–160, 2018.

[24] Manitoba Hydro International Ltd, "Transient Analysis for PSCAD Power System Simulation - USER'S GUIDE - A comprehensive resource for EMTDC," 2018.

[25] B. Gustavsen and H. M. J. De Silva, "Inclusion of rational models in an electromagnetic transients program: Y-parameters, z-parameters, s-parameters, transfer functions," *IEEE Transactions on Power Delivery*, vol. 28, no. 2, pp. 1164–1174, 2013.